Modeling the chemical evolution of ω Centauri using three-dimensional hydrodynamical simulations*

A. Marcolini[1], A. Sollima[2], A. D'Ercole[3], B.K Gibson[1,4] and F. R. Ferraro[2]

[1] *Centre for Astrophysics, University of Central Lancashire, Preston, Lancashire, PR1 2HE, United Kingdom*
[2] *Dipartimento di Astronomia, Università di Bologna, via Ranzani 1, 40127 Bologna, Italy*
[3] *Osservatorio Astronomico di Bologna, via Ranzani 1, 40127 Bologna, Italy*
[4] *School of Physics, University of Sydney, NSW, 2006, Australia*

ABSTRACT

We present a hydrodynamical and chemical model for the globular cluster ω Cen, under the assumption that it is the remnant of an ancient dwarf spheroidal galaxy (dSph), the bulk of which was disrupted and accreted by our Galaxy $\sim$10 Gyr ago. We highlight the very different roles played by Type II and Type Ia supernovae (SNe) in the chemical enrichment of the inner regions of the putative parent dSph. While the SNe II pollute the interstellar medium rather uniformly, the SNe Ia ejecta may remain confined inside dense pockets of gas as long as succesive SNe II explosions spread them out. Stars forming in such pockets have lower α-to-iron ratios than the stars forming elsewhere. Owing to the inhomogeneous pollution by SNe Ia, the metal distribution of the stars in the central region differs substantially from that of the main population of the dwarf galaxy, and resembles that observed in ω Cen. This inhomogeneous mixing is also responsible for a radial segregation of iron-rich stars with depleted [α/Fe] ratios, as observed in some dSphs. Assuming a star formation history of $\sim$1.5 Gyr, our model succeeds in reproducing both the iron and calcium distributions observed in ω Cen and the main features observed in the empirical α/Fe versus Fe/H plane. Finally, our model reproduces the overall spread of the color-magnitude diagram, but fails in reproducing the morphology of the SGB-a and the double morphology of the main sequence. However, the inhomogeneous pollution reduces (but does not eliminate) the need for a significantly enhanced helium abundance to explain the anomalous position of the blue main sequence. Further models taking into account the dynamical interaction of the parent dwarf galaxy with the Milky Way and the effect of AGB pollution will be required.

Key words: hydrodynamics - galaxies: dwarf - galaxies: evolution - globular cluster: ω Centauri - stars: abundances

1 INTRODUCTION

The stellar system ω Cen (NGC 5139) is unique amongst Galactic star clusters in terms of its structure, kinematics, and stellar content. It is the only known globular cluster (GC) showing a clear [Fe/H] spread (Norris et al. 1996, and references therein). Recent photometric surveys have revealed the presence of multiple sequences in its color-magnitude diagram (CMD), indicating a complex star formation history (Cannon & Stobie 1973; Rey et al. 2004; Sollima et al. 2005a). On the basis of the analysis of the red

giant branch (RGB) morphology, three different stellar components have been identified: a dominant metal-poor population ([Fe/H]~ -1.6), an intermediate population spanning the metallicity range $-1.3 <$[Fe/H]< -1.0, and a metal rich component with [Fe/H]~ -0.6 (Pancino et al. 2000).

Peculiarities have also been found along the Main Sequence (MS) of the cluster where an additional blue MS (bMS, comprising $\sim 25\%$ of the cluster's MS stars) running parallel to the dominant sequence (rMS) has been resolved (Anderson 2002; Bedin et al. 2004). In contrast with that predicted by stellar models with canonical chemical abundances, bMS stars show a metallicity a factor of two higher than that of the rMS (Piotto et al. 2005). A large helium overabundance ($\Delta Y \sim 0.15$) in the bMS sequence

---

* Research undertaken as part of the Commonwealth Cosmology Initiative (CCI:www.thecci.org).

has been proposed to explain its anomalous position in the CMD (Norris 2004; Piotto et al. 2005; Sollima et al. 2007). However, such a large helium abundance spread poses serious problems for the overall interpretation of the chemical enrichment history of this stellar system. In fact, no chemical enrichment mechanism is able to produce the huge amount of helium required to reproduce the observed MS morphology without dramatically impacting upon the metal abundance (cf. Karakas et al. 2006a; Sollima et al. 2007; Romano et al. 2007).

Interestingly, Pancino et al. (2002) and Origlia et al. (2003) found that while the metal-poor and intermediate-metallicity stellar populations of ω Cen have the expected α-element overabundance observed in halo and GC stars $\langle [\alpha/\text{Fe}] \rangle \simeq 0.3$ (Edvardsson et al. 1993), the most metal-rich population ([Fe/H]~ -0.6) shows a significantly lower α-enhancement ($\langle [\alpha/\text{Fe}] \rangle = 0.1$). The chemical composition of the former populations requires that at least part of the gas released in the interstellar medium (ISM) by SNe II must have been retained by ω Cen over a relatively short (<1 Gyr) time interval. However, the presence of stars with lower values of [α/Fe] at larger values of [Fe/H] indicates SNe Ia have also likely contributed to the chemical evolution of ω Cen. Since SNe Ia explosions occur over a timescale longer than that of SNe II, the ratio [α/Fe] of the polluted ISM tends to decrease with time as [Fe/H] increases. Although the chemical properties of the stellar populations of ω Cen indicate a prolonged star formation, there is no consensus as to its duration. An age spread of 3-5 Gyr has been claimed to explain the overall trend of α-elements with metallicity (Romano et al. 2007). A somewhat shorter ($<$ 1.5 Gyr) age difference has been suggested by Sollima et al. (2005b), comparing theoretical isochrones with the location of a sample of sub-giant stars with known metallicity.

In any case, the body of evidence collected so far leads to the hypothesis that ω Cen was formerly a larger stellar system, possibly a dwarf galaxy (Hughes & Wallerstein 2000; Dinescu et al. 1999; Majewski et al. 2000; Smith et al. 2000; Gnedin et al. 2002; Bekki & Norris 2006; Romano et al. 2007), that lost most of its stars and gas in the interaction with the Milky Way. Under this hypothesis, self-consistent dynamical models, and coupled N-body + hydrodynamical simulations (Carraro & Lia 2000; Bekki & Freeman 2003; Tsuchiya et al. 2004), succeed in reproducing the main observable characteristics of this system, assuming a total mass for the initial object in the range 10^8-10^9 M$_\odot$. Tidal interaction with the Galaxy, as well as ram pressure stripping by its halo gas, have also been invoked to explain the stellar structure and kinematics of the local dwarf spheroidal galaxies (dSphs), and their lack of gas (e.g. van den Bergh 1994; Mayer et al. 2006). In this scenario ω Cen could retain the ejecta of previous generations of stars and thereby self-enrich throughout its star formation history (SFH).

We propose a model for ω Cen based upon 3D hydrodynamical simulations of an evolving dwarf spheroidal galaxy (see Marcolini et al. 2006). In Section 2, we describe the evolution of ω Cen in the general frame proposed by Marcolini et al. (2006). The general results and the possibility of an extended SFH are discussed in Section 3. Section 4 is devoted to the simulation of the systems' CMDs, while our conclusions are drawn in Section 5.

2   THE MODEL

2.1   Qualitative framework

To fully appreciate the chemical enrichment history of ω Cen it is necessary to understand both its SFH and the associated role of SNe feedback on its dynamical and chemical evolution. Marcolini et al. (2006) provide a useful framework in which to pursue work of this nature, in that their three-dimensional hydrodynamical simulations of isolated dSphs are directly comparable to the objects from which ω Cen has been proposed to have originated. In this study, the authors assumed a prolonged intermittent SFH, tracking the roles of both SNe Ia and SNe II in the chemical enrichment history of the system. These models, although intended to give a general picture of dSphs, were tailored to the Draco dwarf galaxy.

The total energy released by the SNe II explosions is much larger than the binding energy of the gas. However, efficient radiative losses enables the galaxy to retain most of its gas, providing the necessary fuel source for the aforementioned prolonged SFH.

The SNe II are more concentrated toward the galactic centre, where their remnants overlap forming a single cavity composed of a network of tunnels filled by hot rarefied gas. The bulk of the ISM is pushed outward to the edge of the cavity. Once the SNe II cease exploding ($\sim$30 Myr after each star burst episode), the global cavity collapses and the ISM flows back down the potential well, giving rise to a new starburst (see Fig. 3 in Marcolini et al. 2006). In conclusion, the gas content in the centre has an oscillating temporal profile whose period is given by the time interval between two successive starbursts.

Given their lower rate, SNe Ia do not significantly affect the general hydrodynamical behaviour of the ISM, but their role is relevant for the chemical evolution of the stars. Because of the longer timescales over which they contribute, the SNe Ia progenitors produced in previous starbursts continue to explode during the quiescent periods, even after the gas has settled back to the central region. The higher ambient gas density (together with the lower explosion rate) results in SNe Ia remnants being isolated from one another during this phase (see Fig. 14 in Marcolini et al. 2006). As a consequence of this inhomogeneous pollution, stars forming in the regions occupied by SN Ia remnants (hereafter referred to as "SNe Ia pockets") have lower [α/Fe] ratios and higher [Fe/H] ratios than those formed elsewhere. This effect is particularly important for the chemical evolution of the central region, where the SN Ia rate is greater and where SN Ia pockets formed in the outer zones are returned to the galactic centre, with the gas flow during the re-collapse phases. The cycle of expansion and re-collapse experienced by the galactic gas tends to homogenise the ISM and SNe ejecta rather rapidly ($\sim 10^8$ yr).

These authors also found that only $\sim$ 20% of the metals ejected by SNe were present in the region where the stars were assumed to form, despite the absence of a galactic wind. The missing metals were pushed to larger distances by the continuous action of the SN explosions and did not enrich the forming stars (thus mimicking an "outflow").
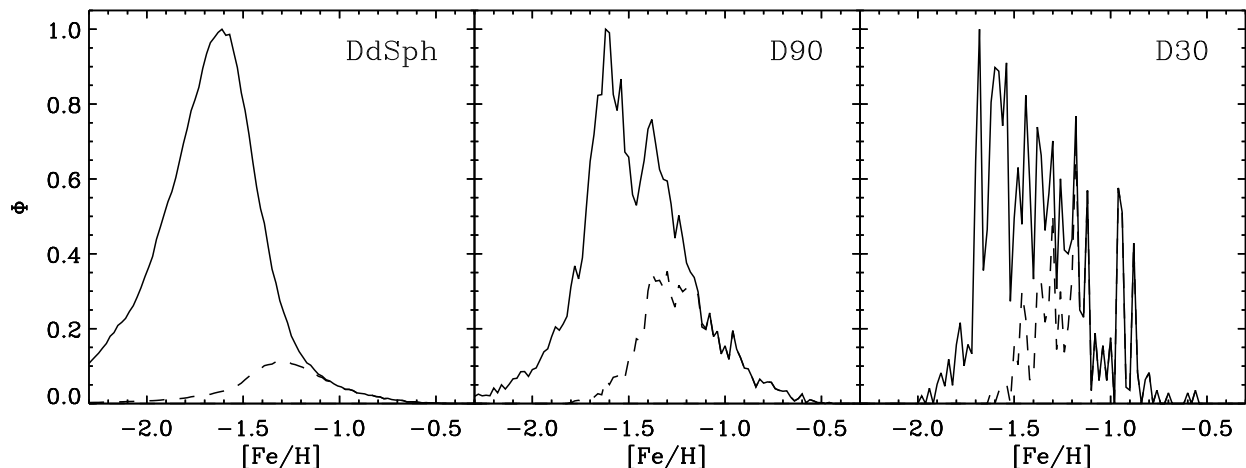
Figure 1. [Fe/H] distribution function of the long lived stars for the whole "entire dSph volume" (left panel; $r_{\star,\mathrm{c}} = 130$ and $r_{\star,\mathrm{t}} = 650$ pc), and two more centrally located regions called "central region" (middle panel, $r_{\star,\mathrm{t}} = 90$ pc) and "nuclear region" (right panel; $r_{\star,\mathrm{t}} = 30$). The dashed lines represent stars with $[\alpha/\mathrm{Fe}] \leqslant 0.2$. See text for more details.

2.2 SNe chemical abundances

The numerical method used to treat the SNe explosions is described in Marcolini et al. (2006). Here we describe briefly the nucleosynthesis prescription assumed in this paper. Nucleosynthesis products of SNe II and SNe Ia are taken from Iwamoto et al. (1999, and references therein). Their Table 3 summarises the mean SN II yields averaged over the $10 - 50$ M$_\odot$ precursors, and the yields for different models of SN Ia (we will refer to their W7 model). We calculate the α-element enrichment by summing the different contributions of O, Mg, Ne, Si, S, Ca, Ti and Ar. We find that a slightly enhanced Ca production (50%) over the mean SNe II value helps to better reconcile model predictions with observations. Note that this increase lies within the uncertainties associated with the different SNe models. These yields depend slightly on metallicity, unless metals are completely absent (Woosley & Weaver 1995; Limongi et al. 2000); we do not consider this dependence because it does not affect the $[\alpha/\mathrm{Fe}]$ features of the stars with $[\mathrm{Fe/H}] > -3$ (Goswami & Prantzos 2000). The adopted yields are listed in Table 1, together with the adopted solar abundances (adopted from Grevesse & Sauval 1998).

2.3 Color-magnitude diagrams

As a first step, in order to simulate the morphology of the CMD we use the evolutionary tracks of Cassisi et al. (2004) and Pietrinferni et al. (2006), calculated for two different α-enhancement levels ($[\alpha/\mathrm{Fe}] = 0.0$ and $[\alpha/\mathrm{Fe}]=+0.4$). As we will show in Sec. 3 a number of stars in our models show $[\alpha/\mathrm{Fe}]$ values that lie outside these limits, especially at sub-solar values of $[\alpha/\mathrm{Fe}]$. In order to take these stars into account, we extrapolated for each metallicity Z the evolutionary tracks down to values of $[\alpha/\mathrm{Fe}]=-0.4$.

For each star, our code stores its iron abundance [Fe/H], its metallicity Z, its α-enhancement $[\alpha/\mathrm{Fe}]$, and the epoch of formation. Then, for each star we randomly extracted 100 masses from a Salpeter (1955) IMF in the mass range

Table 1. Assumed average SNe yields in solar masses[a]

species	SN II[b]	SN Ia[c]	Sun[d]
$M_{\mathrm{tot,ej}}$	17.0	1.4	
M_Z	3.0	1.4	0.016
M_{Fe}	9.07×10^{-2}	0.75	1.23×10^{-3}
M_O	1.80	0.14	7.56×10^{-3}
M_{Mg}	0.12	8.57×10^{-3}	6.45×10^{-4}
M_{Si}	0.12	0.16	6.96×10^{-4}
M_{Ca}	8.80×10^{-3}	1.19×10^{-2}	6.41×10^{-5}
M_α	2.34	0.43	1.12×10^{-2}
$[\alpha/\mathrm{Fe}]$	0.45	-1.20	0

[a] From Iwamoto et al. 1999
[b] Averaged over the progenitor mass range 10-50 M$_\odot$
[c] Model W7
[d] Solar abundances from Grevesse & Sauval (1998).

0.5 M$_\odot$ <M< 0.9 M$_\odot$ and placed them in the theoretical $\log(L/L_\odot)$, $\log T_{\mathrm{eff}}$ plane by means of suitable interpolations of the adopted evolutionary tracks. Luminosities and effective temperatures were transformed into the desired photometric system by interpolation within appropriate tables for photometric conversions (for a detailed description see Cassisi et al. 2004). Following these prescriptions we simulated a CMD of 100,000 stars in the Johnson-Cousin and in the ACS VEGAMAG photometric systems.

In section 4 we will compar our synthetic CMD with the observed CMDs by Sollima et al. (2005a), Ferraro et al. (2004) and Sollima et al. (2007). To convert the absolute magnitudes into the apparent ones, we need to assume a distance modulus and a reddening correction. In the following, we adopt $(m - M)_0 = 13.70$ (Bellazzini et al. 2004; Del Principe et al. 2006), the reddening E(B-V)=0.11 (Lub 2002), the extinction coefficients $A_B = 4.1\ E(B - V)$, $A_V = 3.1\ E(B-V)$, $A_R = 2.32\ E(B-V)$ (Savage & Mathis 1979) for the Johnson-Cousin passbands and $A_{F435W} = 4.02\ E(B - V)$, $A_{F625W} = 2.62\ E(B - V)$ (Sirianni et al.
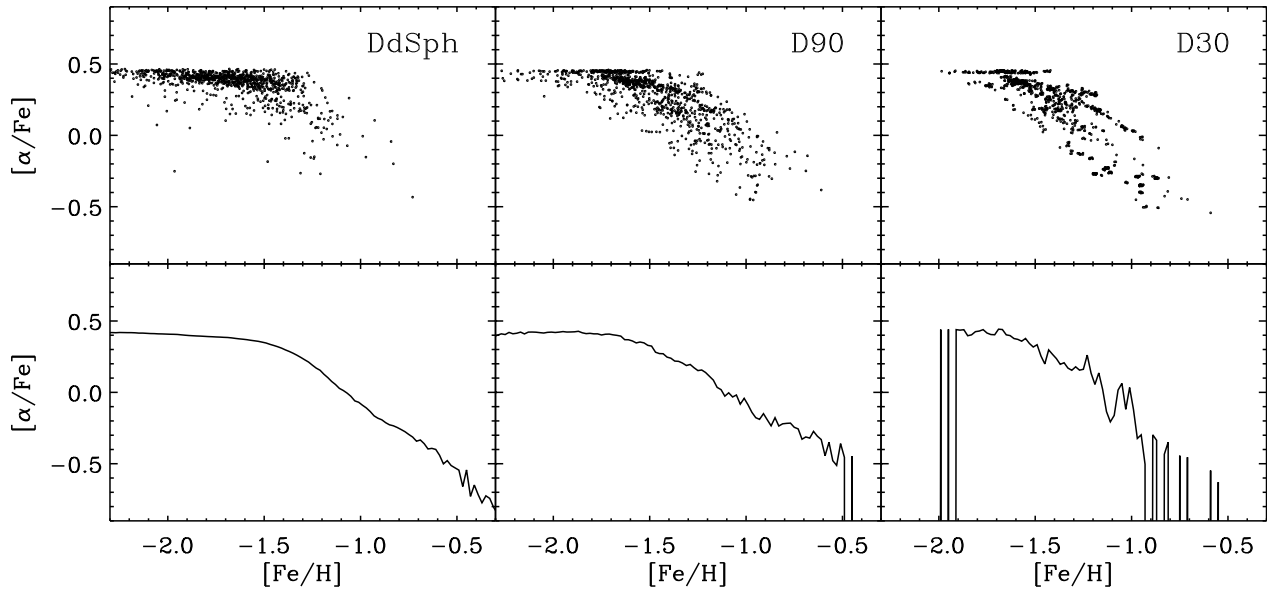
Figure 2. Upper panels: abundance ratio [α/Fe] plotted against [Fe/H] of $N_S = 1000$ sampled stars for the three different regions as in Fig.1. Lower panels: mean values of [α/Fe] for the same stellar sampling.
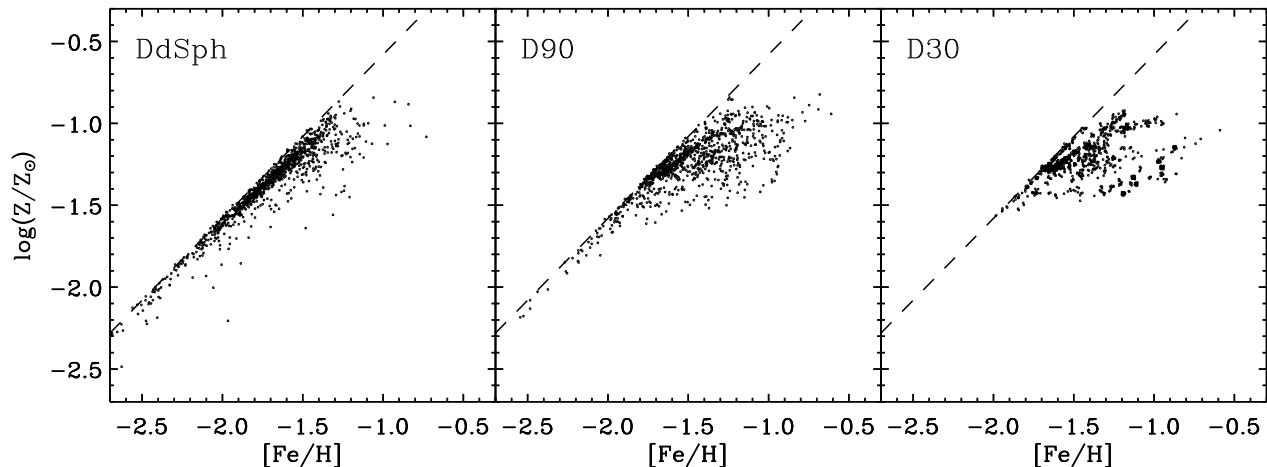

Figure 3. [Fe/H] of $N_S = 1000$ sampled stars plotted against the metallicity Z for the three different regions as in Fig. 1. The dashed line represents the linear relation given by eq. (2) in the case of pure SN II enrichment.

2005) for the ACS passbands. For each star a random photometric error extracted from a Gaussian distribution with σ equal to the average photometric error estimated in that magnitude range by the above authors has been added.

2.4 Adapting the model to ω Centauri

The 3D simulations employed here were generated using the Marcolini et al. (2006) hydrodynamical code. As pointed out in Section 1, in the scenario that assumes ω Cen is the remnant of a dwarf galaxy accreted by the Milky Way, most of the initial mass of the proto-galaxy has been stripped, presumably by the tidal interaction with the Milky Way. Un-

fortunately, our model cannot account for the self-consistent interaction of the proto-galaxy with the Milky Way. Thus, we adopt a model originally tailored to the Draco dSph (see Marcolini et al. 2006), but now focusing our analysis on the central regions of the models - i.e., those regions expected (potentially) to survive as a "globular cluster" like ω Cen.

In the model, the SFH is represented as a sequence of instantaneous star bursts separated by quiescent periods ($\Delta t = 60$ Myr). At the end of the entire star-formation process, nearly 6×10^5 M$_\odot$ of stars have been formed, and 6×10^3 SNe II exploded. The Draco galaxy has a stellar mass content smaller by a factor of 4-8 (e.g. Meylan et al. 1995; van de Ven et al. 2006; Mateo 1998) and a much more
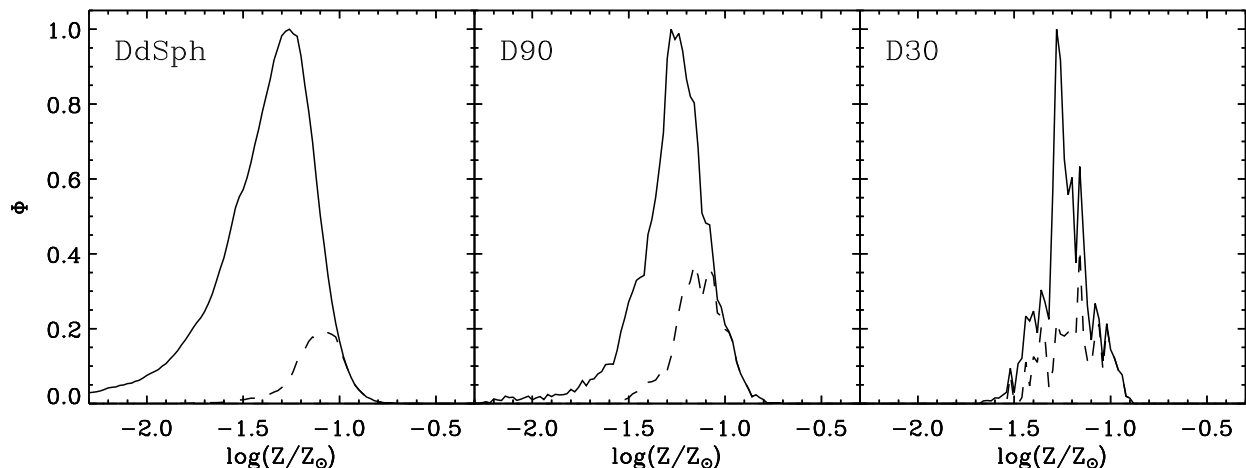
Figure 4. Metallicity (Z) distribution function of the long lived stars for the "entire dSph volume" (left panel), the "central region" (middle panel) and the "nuclear region" as in Fig. 1. The dashed lines represent stars with [Fe/H]$\geqslant -1.4$.

extended stellar distribution than ω Cen. These differences are possibly even more marked if we consider the structure of ω Cen *before* the interaction with the Milky Way. Thus, in order to match the chemical properties of the dominant population of the system, the number of SNe and the initial amount of gas in the "proto" ω Cen have been scaled appropriately, and the star formation suppressed after ~1 Gyr.

ω Cen has a stellar mass content of $\sim 3 \times 10^6$ M$_\odot$ van de Ven et al. (2006) and a radial profile consistent with a King model with $r_c = 4.1$ pc and $r_t = 83$ pc (Ferraro et al. 2006). We followed the chemical evolution of the stellar population of the dSph progenitor in three different regions,, defined as follow: *i*) the "entire dSph volume" with a tidal radius $r_{\star,t} = 650$ pc (see Marcolini et al. 2006 for more details); *ii*) the "central region" within a radius $r_{\star,t} = 90$ pc; and, *iii*) the "nuclear region", with $r_{\star,t} = 30$ pc. These latter two regions are dense enough to survive the tidal disruption incurred through the interaction with the Galaxy, and appear today like a globular cluster. We thus focus our analysis on the central and nuclear regions, and will refer to them as models D90 and D30, respectively.

3   RESULTS

Figure 1 illustrates the [Fe/H] distribution of the long-lived stars (with masses M < 0.9 M$_\odot$) formed over 1 Gyr in the three regions described above. The distribution shown in the left panel is a rather smooth log normal-type distribution, similar to those found in dSphs (e.g. Bellazzini et al. 2002; Babusiaux et al. 2005; Koch et al. 2006; Battaglia et al. 2006; Bosler et al. 2007). The profile in the "rentral region" (middle panel), though, shows a bimodal structure similar to that observed in ω Cen (e.g. Norris et al. 1996; Suntzeff & Kraft 1996), with a maximum at [Fe/H]=-1.6 and a secondary peak at [Fe/H]~ -1.3 accounting for $\sim 25\%$ of the cluster's stellar content. The different shape of the latter's distribution is due to the higher SN Ia rate in this region, as well as to the fact that external iron rich SN Ia pockets converge toward the centre during the re-collapsing

stages of the ISM evolution. The right panel in Fig. 1 shows the distribution in the "nuclear region". The noise present is due to sampling statistics and to the fact that the volume considered is comparable to that of single pockets. In each panel only a negligible fraction ($< 1\%$) of stars has a metallicity [Fe/H]> -0.7.

The upper panels of Fig. 2 show the [α/Fe]-[Fe/H] plane for $N_s = 1000$ sampled stars. As in Fig. 1, the left panel refers to the whole galaxy while the central and the right panels refer to the central and the nuclear regions, respectively. The lower panels represent instead the mean value of [α/Fe]. Because of the SN Ia contribution, the Fe-rich stars are, as expected, α-depleted: we find mean values of $\langle[\alpha/\text{Fe}]\rangle \sim 0.4$ at [Fe/H]$= -1.7$ and $\langle[\alpha/\text{Fe}]\rangle \sim 0.2$ at [Fe/H]$= -1.3$, with a large spread in the [α/Fe] distribution at [Fe/H]> -1.5 .

In general, our mean value of [α/Fe] in the high metallicity regime (Fe/H> -1.0) is slightly smaller than that observed by Smith et al. (2000) and Origlia et al. (2003). This discrepancy is most likely due to the simple form of the SFH we assumed. In Section 3.1 we will show that this discrepancy, as well as the lack of metal-rich ([Fe/H]> -0.7) stars, may be reduced by adopting a more protracted SFH. Indeed, assuming that the star formation can last beyond 1 Gyr at a lower rate, high-metallicity stars ([Fe/H]$\gtrsim -1.3$) may continue to form with high [α/Fe] values because of the freshly-expelled ejecta from recent SNe II explosions.

We must re-iterate the difference between the pollution of iron and that of metals, as a whole. It is clear from Table 1 that the ratio between the iron mass and the mass of all the metals is rather different in the ejecta of the two types of SNe. Thus, when the contribution of the SNe Ia to the ISM pollution becomes relevant, the metal mass fraction Z is not linearly proportional to the amount of iron [Fe/H]. It can be shown that, with our assumptions, it is:

$$Z = 0.015 \times 10^{[Fe/H]} 10^{[\alpha/Fe]} \left[1 + 0.08 \left(2.82 \times 10^{-[\alpha/Fe]} - 1 \right) \right] . \quad (1)$$

Figure 3 shows the log($Z/Z_\odot$)-[Fe/H] diagram for the same sample of stars of Fig. 2. The dashed line represents

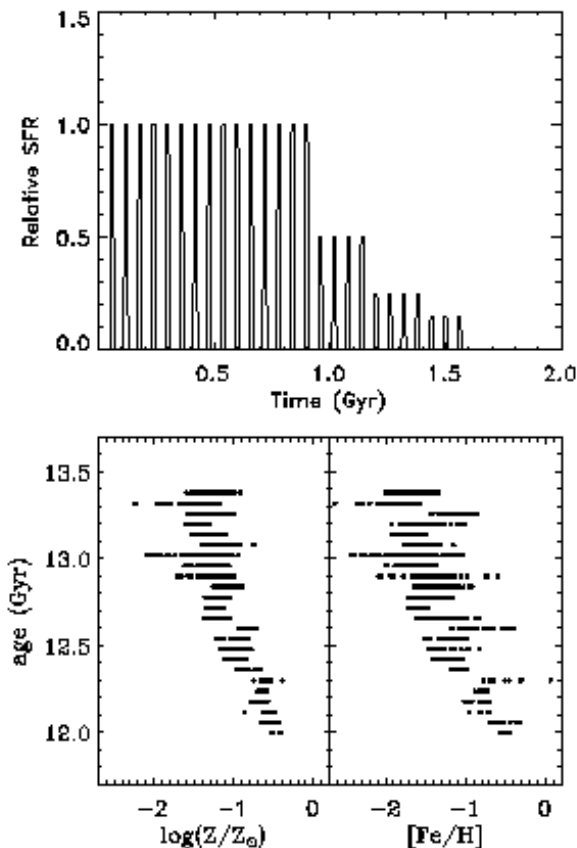**Figure 5.** Upper panel: temporal profile of tha assumed star formation rate in the LONG model. Lower panel: age-Z and age-[Fe/H] distributions of 1000 sampled stars for the D90LONG model. Note the metallicity spread among coeval stars.

the $\log(Z/Z_\odot)$-[Fe/H] relation for stars formed in regions enriched only by SNe II [1]:

$$\log(Z/Z_\odot) = 0.42 + [Fe/H], \qquad (2)$$

assuming $Z_\odot = 0.016$ (Grevesse & Sauval 1998).

The Z distribution for the long-lived stars is plotted in Figure 4. The bimodal structure of the [Fe/H] distribution (see Fig. 1) is now absent and the spread of the Z distribution is similar to the spread of the dominant [Fe/H] poor population. In fact, the number of SNe Ia occurring after 1 Gyr accounts for $\sim 20\%$ of the iron content but only $\sim 1.5\%$ of the produced metal mass. Therefore, in the regions polluted inhomogeneously by SNe Ia, the [Fe/H] ratio increases dramatically, but the metal mass fraction Z remains basically unaffected (c.f. Figure 3). This effect is particularly important in the central regions, where the stars formed in "SNIa pockets" can constitute $\sim 30\%$ of the entire cluster population. In Figure 4 the Z distribution for stars with different iron content is shown for the three regions described in Section 2.4. Note that, in the central regions, Fe-rich ([Fe/H]$\gtrsim -1.4$) and Fe-poor stars span nearly the

same Z range. As we will see in Section 4, this difference influences the position of the stars in the CMD.

3.1 Longer star formation history

As discussed in the previous section only a negligible fraction of stars in our model have a [Fe/H]> -0.7 and the mean value of [α/Fe] in the high metallicity regime ([Fe/H]> -1.0) is slightly smaller than that observed. These discrepancies can be traced to the simple form of the SFH adopted. Indeed, in Section 2.4, we assumed that the star formation of our reference model is suddenly halted after ~ 1 Gyr, due to the interaction with the Milky Way. However, the effect of ram pressure stripping and tidal interactions in more massive dwarf galaxies is likely to be more prolonged, and the time to completely strip the gas from such a system may be of the order of several Gyrs, depending upon the strength of the ram pressure and the orbit of the system (e.g. Marcolini et al. 2003; Mayer et al. 2006).

To explore this possibility, we assumed that after 1 Gyr, the system still forms stars for a further 0.6 Gyr, but at a lower rate. This hypothesis is consistent with the ancient proto-galaxy losing most (but not all) of the gas during its first interaction with the Milky Way. This newly adopted SFH is plotted in the upper panel of Figure 5. In the following, we refer to this model as LONG.

The reduction of the ISM reservoir during this 0.6 Gyr period leads to a corresponding reduction in the rate of the SNe II, whose progenitors are short-lived stars. Conversely, in the same period, the SN Ia rate does not decrease significantly because, in this case, the precursors have longer lifetimes and their explosion rate still depends on the past, higher, SFR. Thus, the rapid gas depletion, together with a rather unaffected iron production, leads to a rapid metal enrichment of the stars forming after the stripping episode, during the final 0.6 Gyr.

As already discussed in Section 2.4, in our original model all the starbursts had the same intensity, and the ISM remains entirely bound to the galaxy. Unfortunately, we cannot mimic the gas stripping by simply reducing artificially the amount of ISM in our model; in this way, in fact, the metals mixed with the ISM would be removed as well and the relative role of SNe II and SNe Ia as polluters would not change. Instead, the metal enrichment is obtained by increasing in time the quantity of SN ejecta present in the simulation; in order to take into account the corresponding drop of the SNII rate due to the decreasing SF over the last 0.6 Gyr, in parallel with the rather unaffected SNIa rate (see above), the relative rates of increasing metal enrichment due to the two SNe types are chosen a posteriori to best fit the data. Not having strong constraints on the orbit of first interaction of the proto-galaxy with the Milky Way (and how the gas stripping proceeded), this remains a necessary free parameter.

In the lower panel of Fig. 5 we plot the age-metallicity diagram for the D90LONG model. As evident, the metallicity increases with time even if a large spread is always present, in agreement with the most recent determinations (e.g. Hilker et al. 2004; Stanford et al. 2006; Villanova et al. 2007). Note that the spread is more evident in the [Fe/H] distribution, as opposed to the Z one, because of the stronger influence of the inhomogeneous SNe Ia enrichment on the

---

[1] This relation is obtained from the previous formula assuming [α/Fe]=+0.45, representative of SNe II ejecta (cf. Table 1)

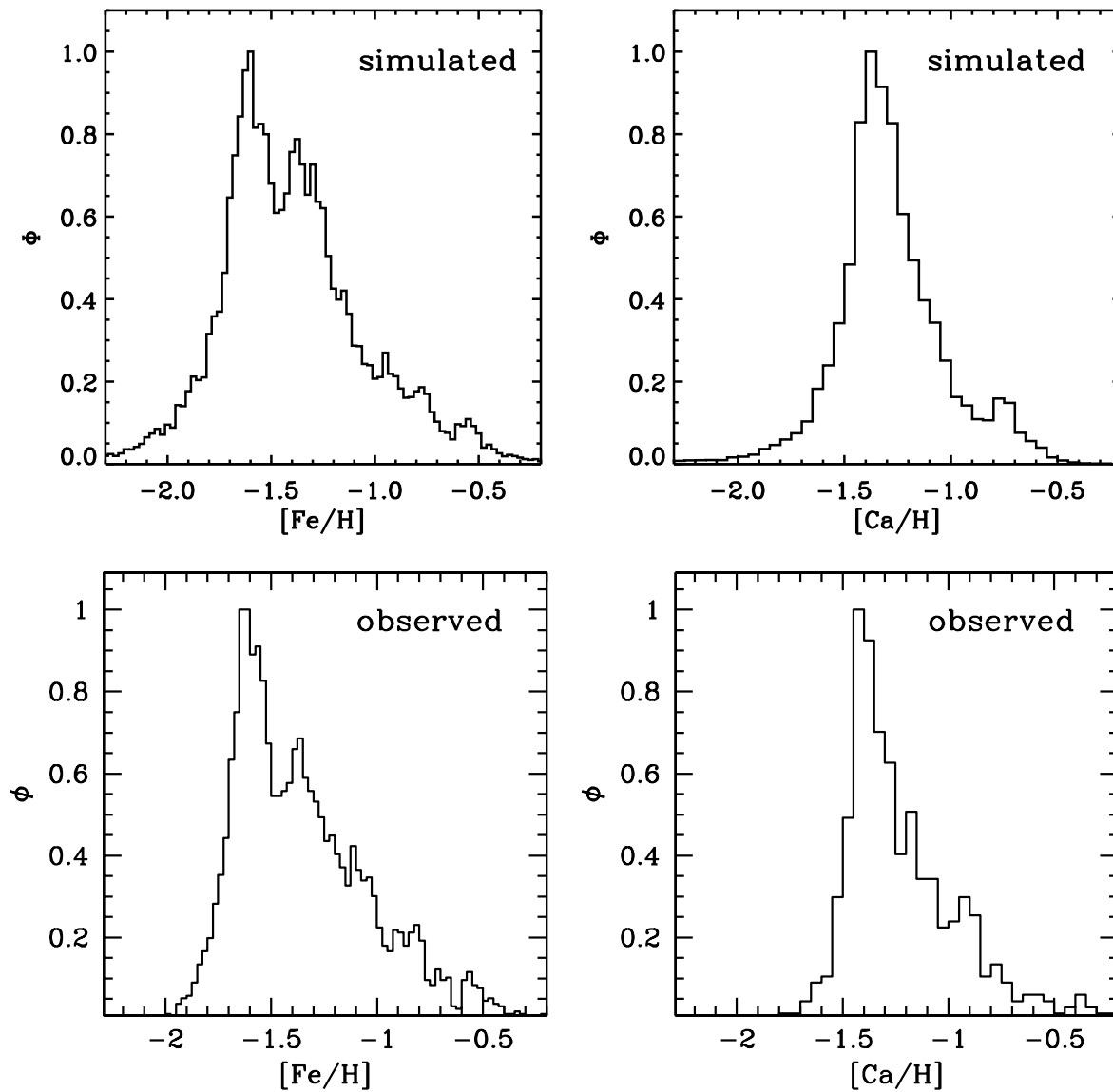**Figure 6.** Left panels: theoretical (D90LONG model) and observative (Sollima et al. 2005a) [Fe/H] distributions of long lived star (upper and lower panels, respectively). Right panels: theoretical and observative (Norris et al. 1996) [Ca/H] distributions of long lived stars (upper and lower panels, respectively).

Fe abundance. We find that we can generate the metallicity distribution functions (and associated observational constraints, as noted below) of ω Cen assuming a SFH lasting 1.6 Gyr, in agreement with the timescale proposed by Ferraro et al. (2004) and Sollima et al. (2005b).

In Figure 6 we show the [Fe/H] and [Ca/H] distributions obtained by the D90LONG model, together with those observed. Comparing the [Fe/H] distribution in the upper-left panel with the corresponding one in Figure 1 we note that the shape of the [Fe/H] distribution remains unaffected at low metallicity ([Fe/H]< −1.2), but for [Fe/H]≳ −1.2 the D90LONG model predicts a larger number of stars and a small peak at [Fe/H]∼ −0.6. The agreement with the [Fe/H] distribution inferred by the observations of Sollima et al. (2005a) is now quite good.

In the same figure we also compare the [Ca/H] distribution found by our model and the one inferred by Norris et al. (1996). Again, the two distributions are in good agreement. Actually, we tend to overestimate the number of stars having [Ca/H]> −0.8, but as stated by Norris et al. (1996), their selection criteria tends to underestimate the number of stars in this range. Note that, contrary to the iron, the amount of calcium ejected by a single SN Ia is comparable to that expelled by a SN II (SN Ia$_{ej,Ca}$/SN II$_{ej,Ca} \sim 1.4$)[2]. Thus, the two peaks visible in the [Fe/H] distribution become nearly indistinguishable in the [Ca/H] distribution.

In Fig. 7 we plot the projected radial distribution of

---

[2] Note that this ratio is ∼ 8 for iron

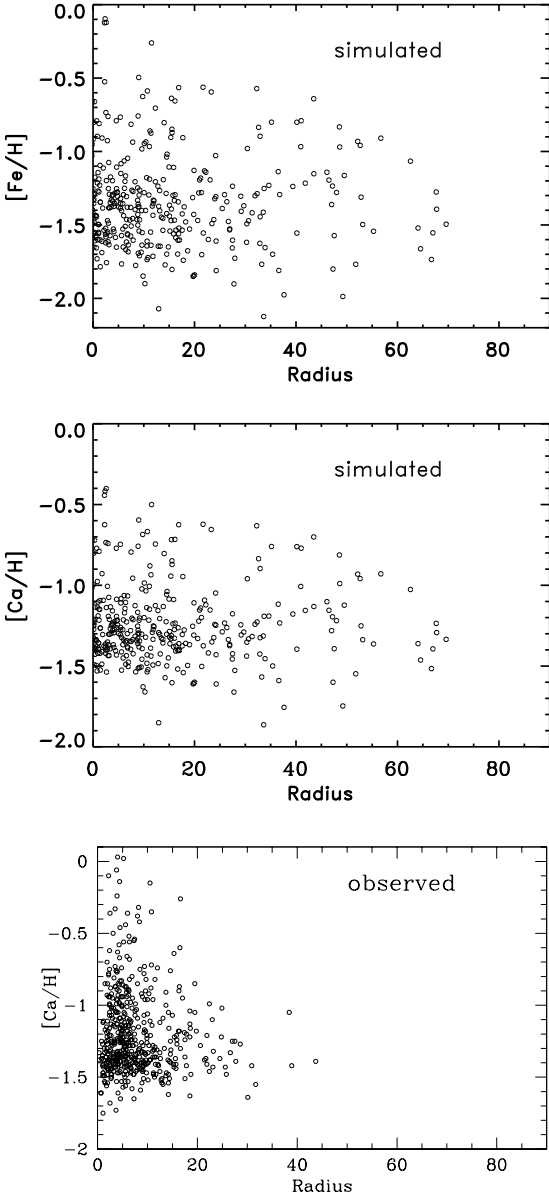**Figure 7.** [Fe/H] (upper panel) and [Ca/H] (middle panel) projected radial distributions of 500 sampled stars for the D90LONG model. The observed [Ca/H] projected radial distributions by Norris et al. (1997) is shown in the bottom panel. Radius is given in pc.

[Fe/H] (upper panel) and [Ca/H] (central panel) for a sample of 500 stars. As already discussed, the most iron-rich stars are more concentrated toward the centre (c.f. Section 2.1). In the bottom panel, the [Ca/H] distribution observed by Norris et al. (1997) is shown. We find good agreement between the observed distribution and that predicted by the D90LONG model.

Figure 8 (left panel) illustrates the $\log(Z)$ distribution predicted by the D90LONG model. The peak at $\log(Z/Z_\odot) = -0.65$ is due to stars born in the final episode of star formation which have $-0.8 \leqslant$ [Fe/H] $\leqslant -0.4$. These stars have ratios [α/Fe] in the range and $-0.3 \leqslant$ [α/Fe] $\leqslant$

+0.3, as shown by the two central panels of Figure 8. Comparing the central panel of this latter figure with the central panels of Figure 2, we note that the mean [α/Fe] values at [Fe/H]=-1.7, -1.3, and -0.6 are now $< $[$\alpha$/Fe]$> \sim$ $+0.4, +0.2$, and $+0.0$, respectively, in good agreement with the values inferred by Origlia et al. (2003). The improvement at higher [Fe/H] is due to the temporal tail of the star formation. Indeed, as the star formation proceeds (though at a lower rate), the new SNe II explosions release fresh α-elements which raise the [α/Fe] ratio of most of the newly-formed stars. Finally, the right panel of Fig. 8 emphasises the dispersion of the stellar metal fraction in the $\log(Z)$-[Fe/H] diagram.

To better compare our model with observations we plot separately in Figure 9 the abundance patterns of several α-elements (O, Mg, Si, and Ca) as predicted by our model, together with a dataset collected from the literature (Francois et al. 1988; Brown & Wallerstein 1993; Norris & Da Costa 1995; Smith et al. 1995, 2000; Pancino et al. 2002; Vanture et al. 2002; Origlia et al. 2003; Villanova et al. 2007). Altough the data are in good agreement, discrepancies as large as 0.5 dex, are occasionally present (for an extensive discussion of this dataset see Romano et al. 2007).

For each α-element we are able to reproduce the general trend of a nearly constant value up to [Fe/H]$\sim$$-1.0$, followed by a slight decrease down to the value [α/Fe]$\sim$$+0$ at [Fe/H]$\sim$$-0.6$. We also simulate satisfactorily the spread of the data and the peculiar stars with sub-solar [α/Fe] (note in particular the agreement between observations of [O/Fe] at [Fe/H]> -1.6 and the model prediction).

An alternative explanation for the O and Mg depletion is the formation of stars from gas polluted by AGB ejecta (c.f. Cottrell & Da Costa 1981). In this contest, self-consistent models of the chemical evolution of the globular cluster NGC 6752 made by Fenner et al. (2004) are not able to reproduce the O depletion, while Mg turns out to be produced rather than destroyed; see also Denissenkov & Herwig (2003) and Karakas et al. (2006b).

The uncertainties that affect the underlying AGB models undermine the reliability of the predictions and may leave room for an AGB solution (Ventura & D'Antona 2005a,b). The choice of convection treatment within the AGB models is particularly important. When convection is modeled more efficiently, deep Hot Bottom Burning can result (Bloecker & Schoenberner 1991, e.g.), with a strong depletion of oxygen and magnesium (e.g. Ventura & D'Antona 2005b,c), while the C+N+O remains constant to within a factor of two. This could help to explain the presence of low oxygen abundance stars in the top right panel of Figure 10.

Since intermediate mass stars (4-8 $M_\odot$) evolve over timescales (30-70 Myr) comparable to that of the peak of SNe Ia activity (in a "burst" environment) we expect that regions inhomogeneously polluted by SN Ia should also be enriched by intermediate-mass AGB stars, complicating the picture. Since AGB stars produces large quantities of helium (up to Y=0.35, e.g. D'Antona et al. 2005) one might expect stars polluted by AGB ejecta to be rich in helium, even if the content hypothesised by several authors to explain the multiple populations in ω Cen (Piotto et al. 2005; Lee et al. 2005; Sollima et al. 2007) and in other GC (D'Antona et al. 2005; Piotto et al. 2007) require that such stars formed
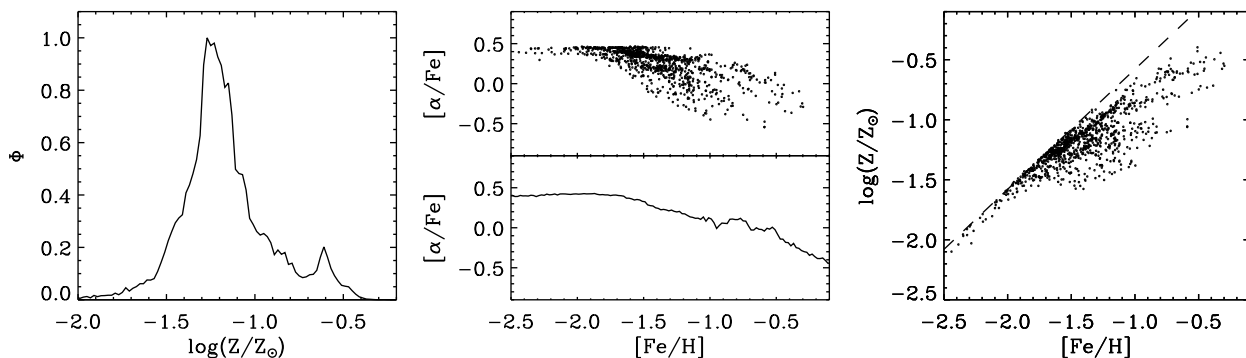
Figure 8. Left panel: $\log(Z)$ stellar distribution. Central panels: $[\alpha/\text{Fe}]$-$[\text{Fe/H}]$ diagram for 1000 sampled stars (top), and $\langle[\alpha/\text{Fe}]\rangle$-$[\text{Fe/H}]$ relation (bottom), where the brakets indicate the mean value of $[\alpha/\text{Fe}]$. Right panel: $\log(Z/Z_\odot)$-$[\text{Fe/H}]$ diagram of 1000 stars sampled in the central region. All the results refer to the model D90LONG

from "pure" AGB ejecta. Regardless, Karakas et al. (2006a) found that only a maximum helium content of Y∼ 0.26 was feasible whitin their models, without violating the observational constraint of near-constant C+N+O.

Finally, ω Cen shows a clear trend of increasing heavy elements produced by s-process synthesis (e.g. Rb, Ba, La, and Nd) with increasing [Fe/H] (Norris & Da Costa 1995; Smith et al. 2000). This is usually interpreted as a sign of the progressive chemical enrichment from 1.5-5 $M_\odot$ AGB stars. The stellar lifetime of stars with mass in these range (~ 1 Gyr for a 2 $M_\odot$ star Schaller et al. 1992) are compatible with the SFH inferred by our study and furthermore the mass reduction in the last ∼600 Myr can aid in the rapid enrichment of these long-lived progenitors' elements. This kind of s-process enrichment trend is peculiar to ω Cen, in comparison with other GC stars.

To be fair, models of the sort described above may only apply to "traditional" GCs, and may not be applicable to ω Cen, but we felt it prudent to at least discussion the feasibility of this scenario here. Recall, ω Cen is the only GC clearly showing a significant spread in iron abundance (as required by SNe Ia enrichment). We are currently developing a new model for canonical GC evolution based upon similar ingredients (Marcolini et al. in preparation).

In conclusion, AGB pollution has certainly occurred at some level within ω Cen, and cannot be ignored. With this in mind, in the next section we test the validity of our model by simulating the CMD of ω Cen and comparing it with observed CMDs from the literature.

4 COMPARING THE COLOR-MAGNITUDE DIAGRAMS

Most of the evidence gathered in the past regarding the metallicity spread, the presence of multiple populations, and the possible helium enhancement in ω Cen have been deduced from the peculiar morphology of different sequences in the CMD. It is interesting to check how our models compare with the most recent and accurate observational data. As pointed out in Section 3, our model predicts a wide spread in the distribution of [Fe/H] as well as [α/Fe]. It has been shown that both [Fe/H] and [α/Fe] produce similar ef-

fects on the stellar isochrones (Salaris et al. 1993; Kim et al. 2002; Cassisi et al. 2004; Pietrinferni et al. 2006, although, see Dotter et al. 2007 for a more thorough discussion of the impact of individual elements on stellar population models). In particular, the low first-ionization potential of Mg, Si and Fe favours the formation of H^- ions that are the main contributors to the mean opacity. Moreover, the increase in the abundances of C, N, O and Ne produces significant change in the opacity and in the efficiency of the CNO nuclear burning that mimic a higher average metallicity Z (Renzini 1977).

In Fig. 10 the color distribution of RGB stars at two different magnitude levels is shown for both the simulated (D30LONG model) and the observed (Sollima et al. 2005a) CMD in the V,B-V plane. The colour distribution of the RGB of ω Cen is well reproduced. The most metal-rich anomalous component (RGB-a, [Fe/H]∼-0.6), well distinguishable in the red part of the CMD of Sollima et al. (2005a), is less defined in our model (although still present) because of the large spread in [α/Fe] ratios predicted at this metallicity. However, given the relative simplicity of the model, we consider the agreement between the simulated and the observed CMD satisfactory.

A behaviour similar to that observed in Fig. 10 is also present in Fig. 11, where our D30LONG model is compared with the ACS CMD by Ferraro et al. (2004) in the sub-giant branch (SGB) region. As can be noted, the observed magnitude spread of the upper part of the SGB, as well as the presence of the anomalous SGB (SGB-a), are accounted for. However, the shape and the slope of the SGB-a are not well reproduced. This effect has been already discussed by Ferraro et al. (2004) and Sollima et al. (2005b, ; and references therein) and could be linked to the possible presence of a significant He overabundance at these metallicities. According to our model, stars lying along this sequence should have a high iron content ([Fe/H]∼ −0.6), in agreement with spectroscopic measurements of stars belonging to this sequence (Hilker et al. 2004; Sollima et al. 2005b; Stanford et al. 2006). It is worth recalling that none of our previous models (DdSph, D90 and D30) reaches such a high metal content. Indeed, this anomalous metal-rich population appears to form in the last ∼0.6 Gyr of evolution of ω Cen.

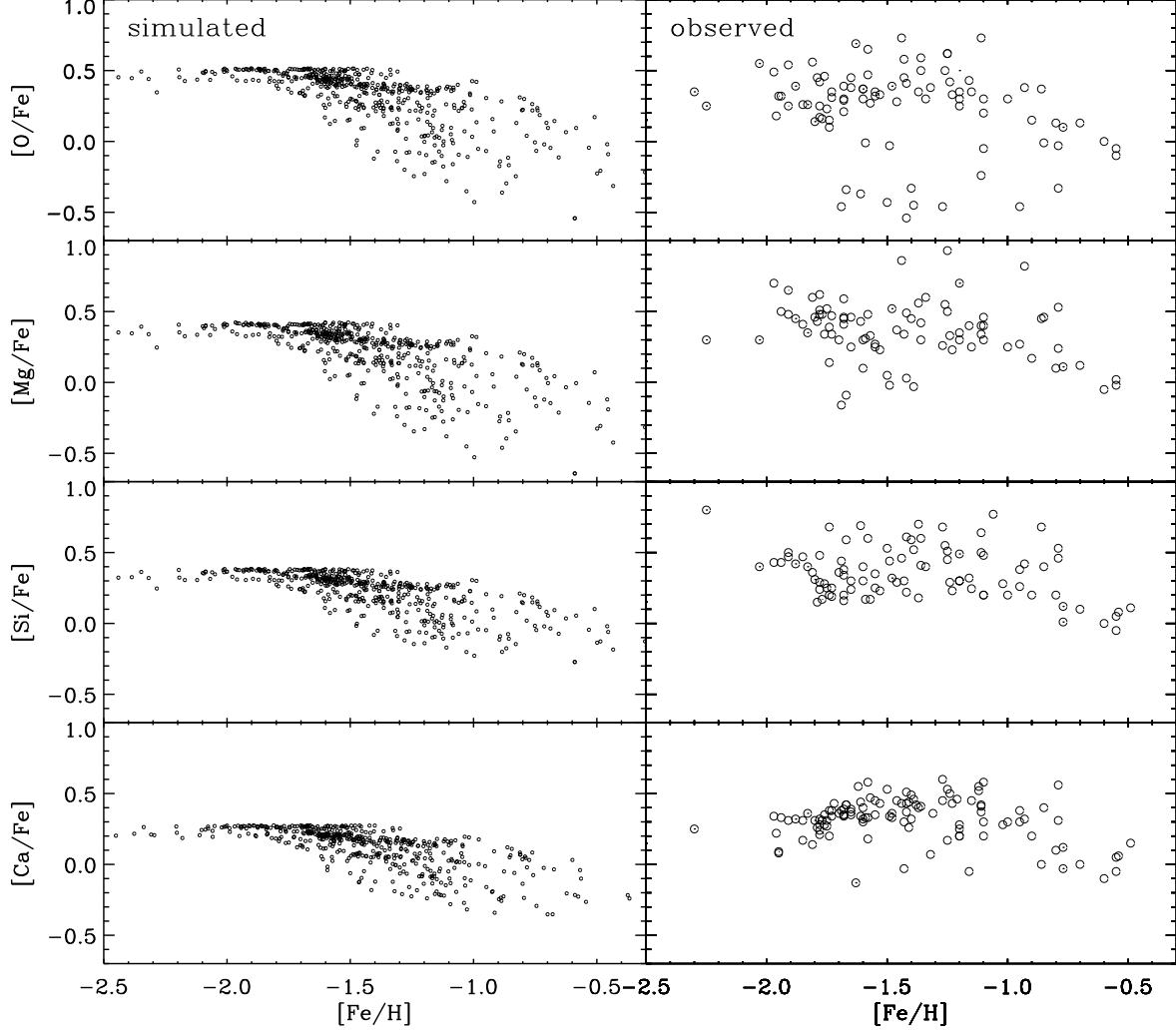Finally, in Fig. 12 we compare our model with the CMD obtained by Sollima et al. (2007) from deep FORS1 observa-

Figure 9. Predicted abundance ratios of several α-elements to iron as a function of [Fe/H] of $N_S = 500$ sampled stars (left panels). Observative data are in the right panels (see text for the references).

tions of the MS of ω Cen. Metal-rich stars ([Fe/H]$\gtrsim -1.4$) are marked as grey points in the synthetic CMD. In the bottom panels, the colour distributions of Fe-poor ([Fe/H]$<$ -1.4) and Fe-rich ([Fe/H]$\gtrsim -1.4$) stars in the simulated CMD and of observed stars are shown. As can be noted, Fe-rich stars are mostly located in the same region of the other Fe-poor stars as expected for two population with similar distributions of Z (see Section 3).

As noted in Section 1, spectroscopic analyses indicate that metal-rich ([Fe/H]~ -1.3) MS stars in ω Cen have been found to lie in the blue portion of the MS, in contradiction with the canonical theoretical models (Piotto et al. 2005). In order to explain the anomalous location of these stars in the CMD, a large helium overabundance has been claimed by several authors (Norris 2004; Piotto et al. 2005; Lee et al. 2005; Sollima et al. 2007). According to our model, the mean

helium abundance remains basically unchanged during the entire process of self-enrichment at any distance from the cluster centre ($\Delta Y < 0.05$). The same conclusion is drawn from recent analytical (ie. without associated dynamical evolution of the gas) galactic chemical evolution models (Romano et al. 2007). Although our model fails to reproduce the MS morphology of ω Cen, the lower mean α-element abundance predicted for the Fe-rich group of stars tends to reduce the color distance between bMS and rMS. According to the theoretical models of Straniero et al. (1997), in this scenario the required amount of helium overabundance to shift the metal-rich ([Fe/H]~ -1.3) MS on the blue side of the dominant Fe-poor cluster MS is reduced by a factor of 40% ($\Delta Y \sim 0.09$).

Finally, in Fig. 13 we plot our full (R,B-R) CMD. The location in the CMD of stars in three different ranges of
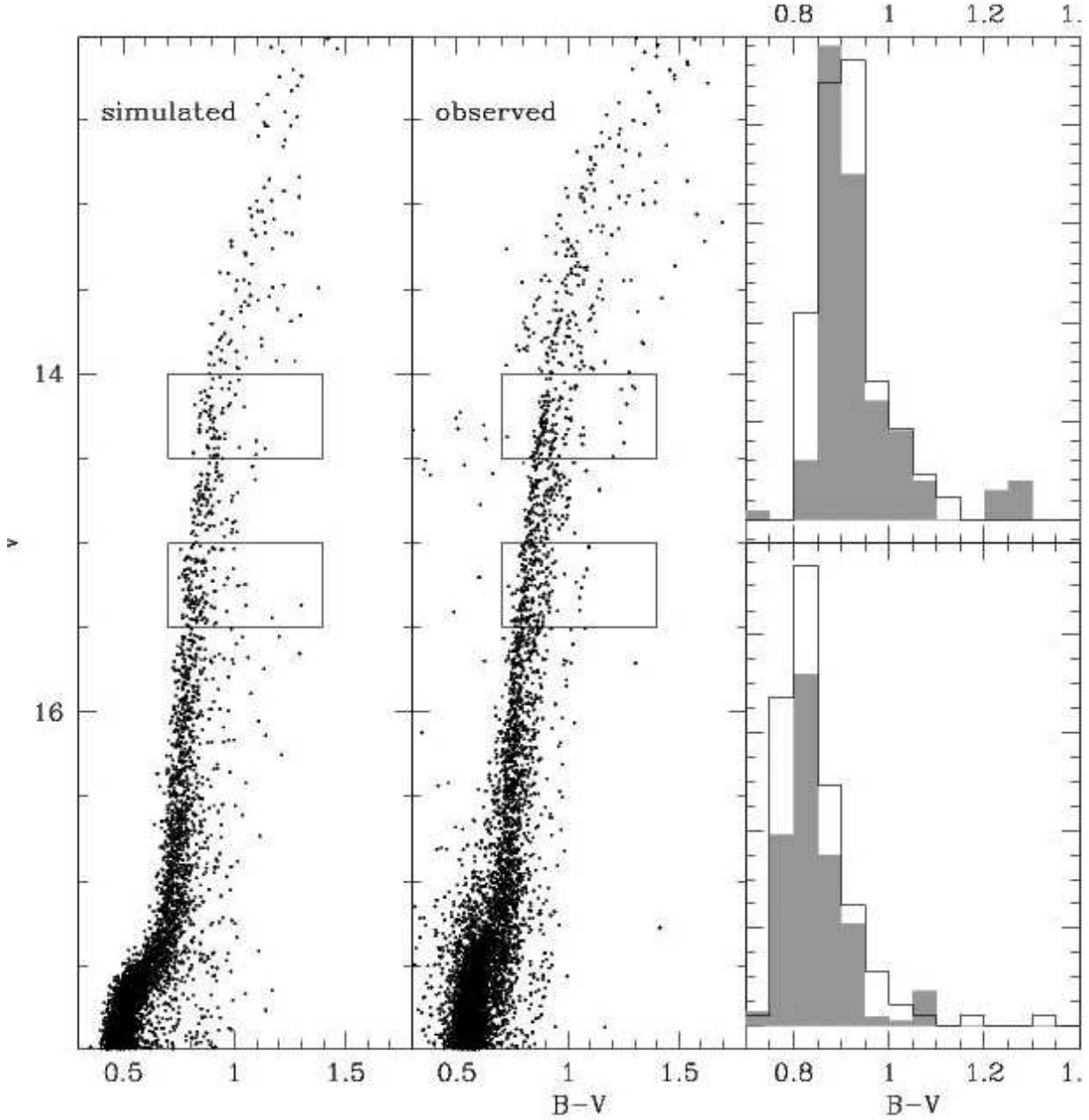
Figure 10. Comparison between the simulated (D30LONG model; left panel) and the observed (from Sollima et al. 2005a; central panel) (V; B-V) CMD of ω Cen. Right panels shows the color histograms between two different V magnitude intervals (indicated by rectangles in the left and central panels) for the observed and simulated (grey histograms) CMD.

[Fe/H] are shown. Note that, although the three groups populate preferentially different regions of the CMD, they partially overlap. As discussed in Section 3, this is due to the fact that the [Fe/H] is not stictly linearly proportional to the metal mass fraction, and stars with the same Z can have different [Fe/H] content. In this picture our model could explain the peculiar position of the outliers observed by Villanova et al. (2007) in their spectroscopic analysis of subgiant stars. These stars have been indeed found to have a [Fe/H]>-1.0 although their position in the CMD would suggest a significant smaller [Fe/H]. The comparison with our

model suggests that the location of these stars in the CMD could be explained if these stars show a significant $[\alpha/Fe]$ depletion.

While a detailed comparison of every aspect of the CMD is beyond the scope of the paper, we have demonstrated that the possibility that ω Cen had its origin in a single progression of star formation and metal enrichment cannot yet be entirely dismissed (cf. Villanova et al. 2007). Our proposed scenario is not meant to be interpreted as the only solution to the problem and to recover all the aspects of the CMD morphology, but neither should it be ignored when
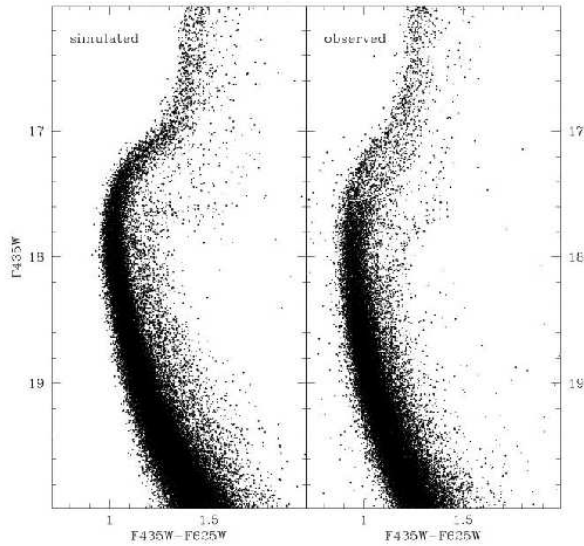
Figure 11. Comparison between the simulated (D30LONG model; left panel) and observed (from Ferraro et al. 2004; right panel) (F625W; F435W-F625W) CMD of ω Cen.

Figure 13. Simulated (R; B-R) CMD of ω Cen (D30LONG model). In the different panels stars with [Fe/H]<-1.4 (left panel), -1.4 <[Fe/H]<-0.8 (central panel) and [Fe/H]>-0.8 (right panel) are marked as black points.

interpreting the MS, SGB and RGB morphologies (it may be that a required solution involving our mechanism alongside that of enhanced helium may be required).

5 DISCUSSION AND CONCLUSIONS

We studied the chemical evolution of the peculiar stellar system ω Cen under the assumption that it represents the nuclear region of a dSph deprived of most of its mass by its interaction with the Milky Way. We based our model on hydrodynamical simulations by Marcolini et al. (2006) describing the evolution of an isolated dSph galaxy. We focused our analysis on the central region of the system, comparing its chemical properties with the observational data available in literature.

We paid particular attention to the different role played by SNe II and SNe Ia in the chemical enrichment of the gas. While the SNe II pollute the ISM rather uniformly, the SN Ia ejecta may remain temporarily confined inside relatively small pockets of gas before being mixed with the ISM. The stars forming in such pockets have lower [α/Fe] ratios than the stars forming elsewhere which show a significant α-enhancement ($\langle[\alpha/\text{Fe}]\rangle \geqslant 0.35$). α-depleted stars represent only $\sim$7% of the entire dSph stellar population, but their fraction rises up to $\sim$30% in the central region. This difference depends on the hydrodynamical evolution, as well as on the higher rate of SNe Ia in the central regions of the system. As a consequence, the chemical properties of the stars forming in the nuclear region of a dSph differ substantially from those of the main dSph population, and can resemble those observed in ω Cen.

The Z and [Fe/H] distributions of ω Cen have been reproduced assuming that 85% of the stars were born within 1 Gyr (in a sequence of equal-intensity starbursts) and the remaining fraction formed during the subsequent 0.6 Gyr at a lower rate (owing to the interaction with the Galaxy).
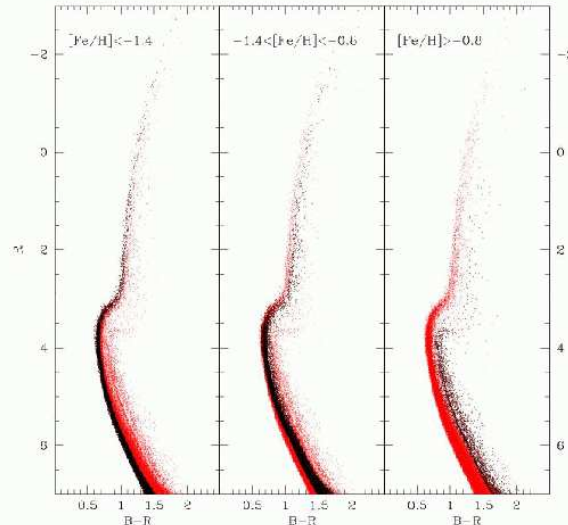
The stars created in this last period show a rapid increase of their [Fe/H] because of the rapid reduction of the gas mass content as a consequence of the interaction between the dSph and the Milky Way.

The first constraint against wich our model has been tested is that of the [Fe/H] and [Ca/H] distributions of the stars observed in ω Cen (Norris et al. 1996; Sollima et al. 2005a). The inhomogeneous mixing of the metals ejected by SNe Ia naturally explains the observed multimodal distributions, as well as their radial profile.

From accurate CMD simulations, we compared the morphology of the evolutionary sequences with that predicted by our model. Our model is successful in reproducing the overall spread in the RGB and SGB morphology, but fails to mimic the SGB-a morphology. It also fails to reproduce the bimodal MS observed in this cluster. However, due to the relationship between the [α/Fe] and [Fe/H] ratios in the SNe Ia pockets, the discrepancy between the predicted and observed location of the bMS component can be ameliorated by requiring a reduced level to the helium overabundance ($\Delta Y \sim 0.09$) usually invoked (Norris 2004; Piotto et al. 2005; Sollima et al. 2007).

A further test able to validate the inhomogeneous pollution expected by our model should be the observation in ω Cen of some stars with sub-solar [α/Fe] ratios (at [Fe/H]$\geqslant$ -1.5). Note that stars with such a peculiar abundance patterns have already been observed in the centre of some dSphs like Sagittarius (Bonifacio et al. 2004; Monaco et al. 2005; McWilliam & Smecker-Hane 2005; Sbordone et al. 2007), Draco (Shetrone et al. 2001) ,Fornax and Sculptor (Venn & Hill 2005; Tolstoy et al. 2006).

We note that in order to realise our synthetic CMDs, we utilised evolutionary tracks (Cassisi et al. 2004; Pietrinferni et al. 2006) calculated for two different α-enhancement levels ([α/Fe]=+0.0 and [α/Fe]=+0.4). We then extrapolated down to the ratio [α/Fe]=-0.4 (for each
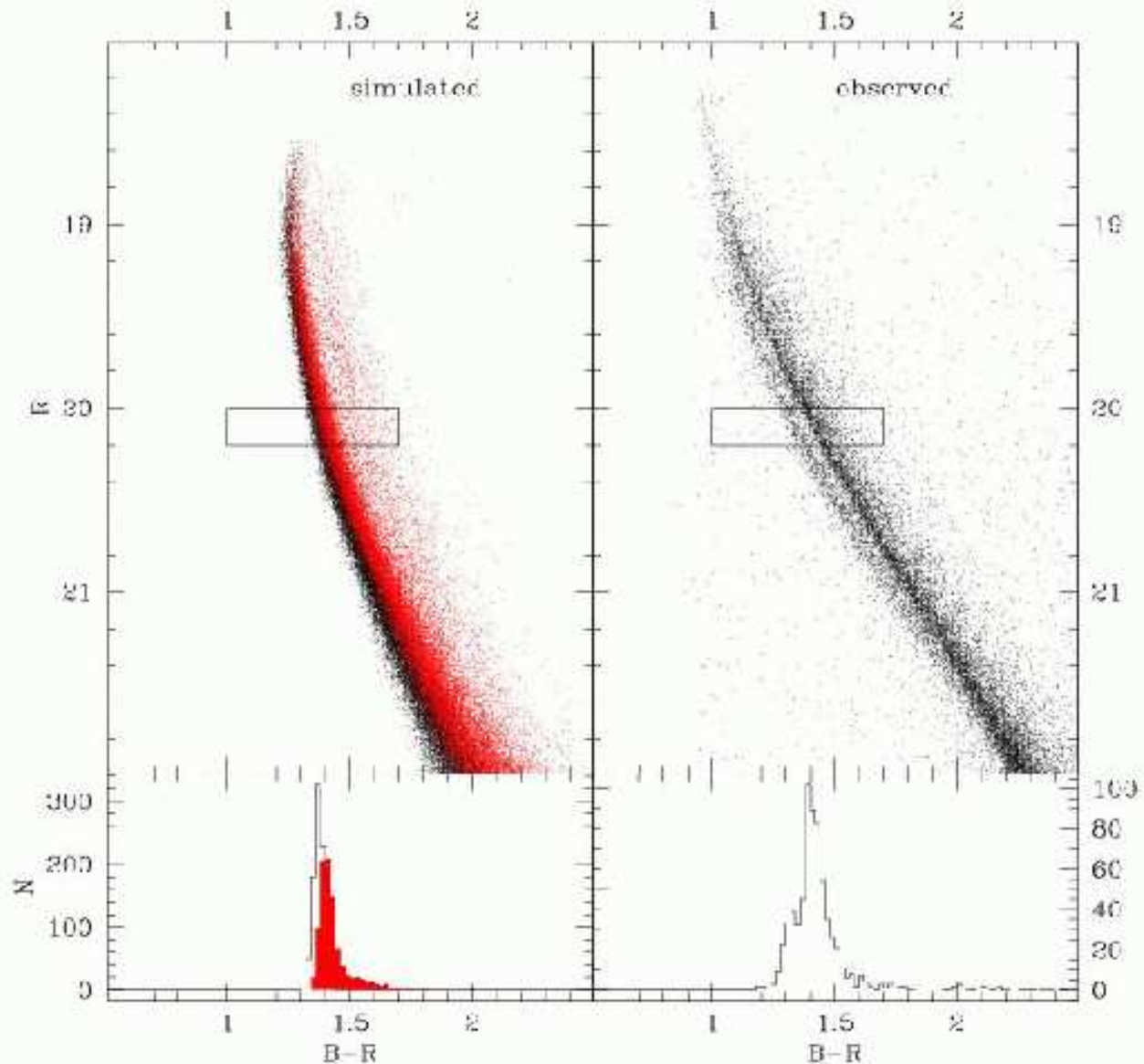
Figure 12. Comparison between the simulated (D30LONG model; upper left panel) and observed (from Sollima et al. 2007; upper right panel) (R; B-R) CMD of ω Cen. Grey points in the left panel marks stars with [Fe/H]> -1.4. In the bottom panels the MS colour histograms calculated at $20 < R < 20.2$ are shown.

Z value) in order to take into account the entire [α/Fe] range covered by the stars in our model. Unfortunatelty, most of these stars do not have solar-scaled abundances, as assumed in the utilised isochrones. Tracks taking into account the relation among Z, [Fe/H] and [α/Fe] given by equation (1) would be desirable to obtain more realistic tests. Moreover, further models taking into account the dynamical interaction of the parent dwarf galaxy with the Milky Way and the effect of AGB pollution will be required.

ACKNOWLEDGMENTS

REFERENCES

Anderson J., 2002, in Astronomical Society of the Pacific Conference Series, Vol. 265, Omega Centauri, A Unique

Window into Astrophysics, van Leeuwen F., Hughes J. D., Piotto G., eds., p. 87

Babusiaux C., Gilmore G., Irwin M., 2005, MNRAS, 359, 985

Battaglia G., Tolstoy E., Helmi A., Irwin M. J., Letarte B., Jablonka P., Hill V., Venn K. A., Shetrone M. D., Arimoto N., Primas F., Kaufer A., Francois P., Szeifert T., Abel T., Sadakane K., 2006, A&A, 459, 423

Bedin L. R., Piotto G., Anderson J., Cassisi S., King I. R., Momany Y., Carraro G., 2004, ApJ, 605, L125

Bekki K., Freeman K. C., 2003, MNRAS, 346, L11

Bekki K., Norris J. E., 2006, ApJ, 637, L109

Bellazzini M., Ferraro F. R., Origlia L., Pancino E., Monaco L., Oliva E., 2002, AJ, 124, 3222

Bellazzini M., Ferraro F. R., Sollima A., Pancino E., Origlia L., 2004, A&A, 424, 199

Bloecker T., Schoenberner D., 1991, A&A, 244, L43

Bonifacio P., Sbordone L., Marconi G., Pasquini L., Hill V., 2004, A&A, 414, 503

Bosler T. L., Smecker-Hane T. A., Stetson P. B., 2007, MNRAS, 378, 318

Brown J. A., Wallerstein G., 1993, AJ, 106, 133

Cannon R. D., Stobie R. S., 1973, MNRAS, 162, 207

Carraro G., Lia C., 2000, A&A, 357, 977

Cassisi S., Salaris M., Castelli F., Pietrinferni A., 2004, ApJ, 616, 498

Cottrell P. L., Da Costa G. S., 1981, ApJ, 245, L79

D'Antona F., Bellazzini M., Caloi V., Pecci F. F., Galleti S., Rood R. T., 2005, ApJ, 631, 868

Del Principe M., Piersimoni A. M., Storm J., Caputo F., Bono G., Stetson P. B., Castellani M., Buonanno R., Calamida A., Corsi C. E., Dall'Ora M., Ferraro I., Freyhammer L. M., Iannicola G., Monelli M., Nonino M., Pulone L., Ripepi V., 2006, ApJ, 652, 362

Denissenkov P. A., Herwig F., 2003, ApJ, 590, L99

Dinescu D. I., van Altena W. F., Girard T. M., López C. E., 1999, AJ, 117, 277

Dotter A., Chaboyer B., Ferguson J. W., Lee H. ., Worthey G., Baron E., Jevremovic D., 2007, astro-ph/07060808

Edvardsson B., Andersen J., Gustafsson B., Lambert D. L., Nissen P. E., Tomkin J., 1993, A&AS, 102, 603

Fenner Y., Campbell S., Karakas A. I., Lattanzio J. C., Gibson B. K., 2004, MNRAS, 353, 789

Ferraro F. R., Sollima A., Pancino E., Bellazzini M., Straniero O., Origlia L., Cool A. M., 2004, ApJ, 603, L81

Ferraro F. R., Sollima A., Rood R. T., Origlia L., Pancino E., Bellazzini M., 2006, ApJ, 638, 433

Francois P., Spite M., Spite F., 1988, A&A, 191, 267

Gnedin O. Y., Zhao H., Pringle J. E., Fall S. M., Livio M., Meylan G., 2002, ApJ, 568, L23

Goswami A., Prantzos N., 2000, A&A, 359, 191

Grevesse N., Sauval A. J., 1998, Space Science Reviews, 85, 161

Hilker M., Kayser A., Richtler T., Willemsen P., 2004, A&A, 422, L9

Hughes J., Wallerstein G., 2000, AJ, 119, 1225

Iwamoto K., Brachwitz F., Nomoto K., Kishimoto N., Umeda H., Hix W. R., Thielemann F.-K., 1999, ApJS, 125, 439

Karakas A. I., Fenner Y., Sills A., Campbell S. W., Lattanzio J. C., 2006a, ApJ, 652, 1240

Karakas A. I., Lugaro M., Ugalde C., Wiescher M., Görres J., 2006b, New Astronomy Review, 50, 500

Kim Y.-C., Demarque P., Yi S. K., Alexander D. R., 2002, ApJS, 143, 499

Koch A., Grebel E. K., Wyse R. F. G., Kleyna J. T., Wilkinson M. I., Harbeck D. R., Gilmore G. F., Evans N. W., 2006, AJ, 131, 895

Lee Y.-W., Joo S.-J., Han S.-I., Chung C., Ree C. H., Sohn Y.-J., Kim Y.-C., Yoon S.-J., Yi S. K., Demarque P., 2005, ApJ, 621, L57

Limongi M., Straniero O., Chieffi A., 2000, ApJS, 129, 625

Lub J., 2002, in ASP Conf. Ser. 265: Omega Centauri, A Unique Window into Astrophysics, van Leeuwen F., Hughes J. D., Piotto G., eds., p. 95

Majewski S. R., Patterson R. J., Dinescu D. I., Johnson W. Y., Ostheimer J. C., Kunkel W. E., Palma C., 2000, in Liege International Astrophysical Colloquia, Noels A., Magain P., Caro D., Jehin E., Parmentier G., Thoul A. A., eds., p. 619

Marcolini A., Brighenti F., D'Ercole A., 2003, MNRAS, 345, 1329

Marcolini A., D'Ercole A., Brighenti F., Recchi S., 2006, MNRAS, 371, 643

Mateo M. L., 1998, ARA&A, 36, 435

Mayer L., Mastropietro C., Wadsley J., Stadel J., Moore B., 2006, MNRAS, 369, 1021

McWilliam A., Smecker-Hane T. A., 2005, in Astronomical Society of the Pacific Conference Series, Vol. 336, Cosmic Abundances as Records of Stellar Evolution and Nucleosynthesis, Barnes III T. G., Bash F. N., eds., p. 221

Meylan G., Mayor M., Duquennoy A., Dubath P., 1995, A&A, 303, 761

Monaco L., Bellazzini M., Bonifacio P., Ferraro F. R., Marconi G., Pancino E., Sbordone L., Zaggia S., 2005, A&A, 441, 141

Norris J. E., 2004, ApJ, 612, L25

Norris J. E., Da Costa G. S., 1995, ApJ, 447, 680

Norris J. E., Freeman K. C., Mayor M., Seitzer P., 1997, ApJ, 487, L187

Norris J. E., Freeman K. C., Mighell K. J., 1996, ApJ, 462, 241

Origlia L., Ferraro F. R., Bellazzini M., Pancino E., 2003, ApJ, 591, 916

Pancino E., Ferraro F. R., Bellazzini M., Piotto G., Zoccali M., 2000, ApJ, 534, L83

Pancino E., Pasquini L., Hill V., Ferraro F. R., Bellazzini M., 2002, ApJ, 568, L101

Pietrinferni A., Cassisi S., Salaris M., Castelli F., 2006, ApJ, 642, 797

Piotto G., Bedin L. R., Anderson J., King I. R., Cassisi S., Milone A. P., Villanova S., Pietrinferni A., Renzini A., 2007, ApJ, 661, L53

Piotto G., Villanova S., Bedin L. R., Gratton R., Cassisi S., Momany Y., Recio-Blanco A., Lucatello S., Anderson J., King I. R., Pietrinferni A., Carraro G., 2005, ApJ, 621, 777

Renzini A., 1977, in Saas-Fee Advanced Course 7: Advanced Stages in Stellar Evolution, Bouvier P., Maeder A., eds., p. 151

Rey S.-C., Lee Y.-W., Ree C. H., Joo J.-M., Sohn Y.-J., Walker A. R., 2004, AJ, 127, 958

Romano D., Matteucci F., Tosi M., Pancino E., Bellazzini

M., Ferraro F. R., Limongi M., Sollima A., 2007, MNRAS, 69

Salaris M., Chieffi A., Straniero O., 1993, ApJ, 414, 580

Savage B. D., Mathis J. S., 1979, ARA&A, 17, 73

Sbordone L., Bonifacio P., Buonanno R., Marconi G., Monaco L., Zaggia S., 2007, A&A, 465, 815

Schaller G., Schaerer D., Meynet G., Maeder A., 1992, A&AS, 96, 269

Shetrone M. D., Côté P., Sargent W. L. W., 2001, ApJ, 548, 592

Sirianni M., Jee M. J., Benítez N., Blakeslee J. P., Martel A. R., Meurer G., Clampin M., De Marchi G., Ford H. C., Gilliland R., Hartig G. F., Illingworth G. D., Mack J., McCann W. J., 2005, PASP, 117, 1049

Smith V. V., Cunha K., Lambert D. L., 1995, AJ, 110, 2827

Smith V. V., Suntzeff N. B., Cunha K., Gallino R., Busso M., Lambert D. L., Straniero O., 2000, AJ, 119, 1239

Sollima A., Ferraro F. R., Bellazzini M., Origlia L., Straniero O., Pancino E., 2007, ApJ, 654, 915

Sollima A., Ferraro F. R., Pancino E., Bellazzini M., 2005a, MNRAS, 357, 265

Sollima A., Pancino E., Ferraro F. R., Bellazzini M., Straniero O., Pasquini L., 2005b, ApJ, 634, 332

Stanford L. M., Da Costa G. S., Norris J. E., Cannon R. D., 2006, ApJ, 647, 1075

Straniero O., Chieffi A., Limongi M., 1997, ApJ, 490, 425

Suntzeff N. B., Kraft R. P., 1996, AJ, 111, 1913

Tolstoy E., Hill V., Irwin M., Helmi A., Battaglia G., Letarte B., Venn K., Jablonka P., Shetrone M., Arimoto N., Abel T., Primas F., Kaufer A., Szeifert T., Francois P., Sadakane K., 2006, The Messenger, 123, 33

Tsuchiya T., Korchagin V. I., Dinescu D. I., 2004, MNRAS, 350, 1141

van de Ven G., van den Bosch R. C. E., Verolme E. K., de Zeeuw P. T., 2006, A&A, 445, 513

van den Bergh S., 1994, ApJ, 428, 617

Vanture A. D., Wallerstein G., Suntzeff N. B., 2002, ApJ, 569, 984

Venn K. A., Hill V., 2005, in IAU Symposium, Vol. 228, From Lithium to Uranium: Elemental Tracers of Early Cosmic Evolution, Hill V., François P., Primas F., eds., pp. 513–518

Ventura P., D'Antona F., 2005a, A&A, 431, 279

—, 2005b, A&A, 439, 1075

—, 2005c, ApJ, 635, L149

Villanova S., Piotto G., King I. R., Anderson J., Bedin L. R., Gratton R. G., Cassisi S., Momany Y., Bellini A., Cool A. M., Recio-Blanco A., Renzini A., 2007, ApJ, 663, 296

Woosley S. E., Weaver T. A., 1995, ApJS, 101, 181